HHS Public Access

Author manuscript

Osteoarthritis Cartilage. Author manuscript; available in PMC 2020 June 01.

Published in final edited form as:

Osteoarthritis Cartilage. 2019 June ; 27(6): 956–964. doi:10.1016/j.joca.2019.01.013.

Nutrient supply and nucleus pulposus cell function: effects of the transport properties of the cartilage endplate and potential implications for intradiscal biologic therapy

Jason Wong[†,§], **Sara L. Sampson**[†,§], **Hildegarde Bell-Briones**[†], **Ann Ouyang**[†], **Ann A. Lazar**[‡,‖], **Jeffrey C. Lotz**[†], and **Aaron J. Fields**[†,*]

[†]Department of Orthopaedic Surgery, University of California San Francisco

[‡]Department of Preventative and Restorative Dental Sciences, University of California San Francisco

[‖]Department of Epidemiology and Biostatistics, University of California San Francisco

[§]These authors contributed equally to this work

Abstract

Objective: Intradiscal biologic therapy is a promising strategy for managing intervertebral disc degeneration. However, these therapies require a rich nutrient supply, which may be limited by the transport properties of the cartilage endplate (CEP). This study investigated how fluctuations in CEP transport properties impact nutrient diffusion and disc cell survival and function.

Design: Human CEP tissues harvested from six fresh cadaveric lumbar spines (38–66 years old) were placed at the open sides of diffusion chambers. Bovine nucleus pulposus (NP) cells cultured inside the chambers were nourished exclusively by nutrients diffusing through the CEP tissues. After 72 hours in culture, depth-dependent NP cell viability and gene expression were measured, and related to CEP transport properties and biochemical composition determined using fluorescence recovery after photobleaching and Fourier transform infrared spectroscopy.

Results: Solute diffusivity varied nearly 4-fold amongst the CEPs studied, and chambers with the least permeable CEPs appeared to have lower aggrecan, collagen-2, and matrix metalloproteinase-2 gene expression, as well as a significantly shorter viable distance from the CEP/nutrient interface. Increasing chamber cell density shortened the viable distance; however, this effect was lost for low-diffusivity CEPs, which suggests that these CEPs may not provide

[*]**Address for reprints and correspondence:** Aaron J. Fields, Ph.D., 513 Parnassus Avenue, S-1161 Box 0514, San Francisco, CA 94143-0514, Tel: + 1 (415) 476-0960, Fax: + 1 (415) 476-1128.

Author contributions

JW, HB, SLS, AO and AJF performed the experiments. AAL and AJF performed the statistical modeling. All authors were involved with analysis and interpretation of the data. JW, SLS, AAL, and AJF wrote the manuscript. All authors revised and approved the final manuscript. AJF conceived, designed, and obtained funding for the study.

Conflict of interest

None.

enough nutrient diffusion to satisfy cell demands. Solute diffusivity in the CEP was associated with biochemical composition: low-diffusivity CEPs had greater amounts of collagen and aggrecan, more mineral, and lower cross-link maturity.

Conclusions: CEP transport properties dramatically affect NP cell survival/function. Degeneration-related CEP matrix changes could hinder the success of biologic therapies that require increased nutrient supply.

Keywords

cartilage endplate; disc degeneration; Fourier transform infrared imaging; nutrient transport; nucleus pulposus cell; low back pain

Introduction

Disc degeneration is a chronic matrix remodeling process that underlies several painful spinal disorders. Current medical interventions are surgical in nature and are aimed at removing potential sources of pain and restoring biomechanical function. Unfortunately, these invasive procedures are often unsuccessful, which motivates development of noninvasive alternatives. One promising strategy is intradiscal biologic therapy, which strives to regenerate the disc by: implanting new cells to produce matrix lost during degeneration[1]; or by injecting genes[2], growth factors[3], or other small molecules[4,5] meant to increase matrix production and reduce catabolism or inflammation. However, increasing cell number or metabolism raises nutrient demand[6], which may not be sustainable in the avascular degenerated disc[7,8]. Determining the factors that influence nutrient transport to the disc cells could enhance development of effective intradiscal therapies, uncover diagnostic targets for selecting ideal discs for treatment, and inform new strategies for improving disc nutrition.

Cells inside the nucleus pulposus (NP) mainly rely on nutrient transport to and from the vertebral capillaries[9,10], which can be compromised by several factors. The vertebral capillaries penetrate pores in the bony endplate and terminate adjacent to the cartilage endplate[11,12] (CEP; Figure 1). Pores in the bony endplate could be occluded during age-related sclerosis[13]; yet, there is also evidence that bony endplate porosity increases with age[14,15]. On the other hand, CEP permeability is at least an order of magnitude lower than bony endplate permeability[16,17], which suggests that the solutes' ability to penetrate and diffuse through the CEP is the primary factor that controls the amount of nutrients and metabolites entering and exiting the disc. Moreover, CEP transport properties may be impaired by degenerative changes to the cartilage matrix[18,19], such as calcification[20,21] and dehydration[22]. However, because it is difficult to isolate the effects of CEP transport properties on nutrient diffusion and disc cell survival, the clinical relevance of deficits in CEP transport properties remains unknown.

To address these issues, we used *in vitro* diffusion chambers to test how human CEPs with a wide range of transport properties impact NP cell function. Our hypothesis was that CEPs with low solute diffusivity significantly reduce NP cell viability and function compared to CEPs with high solute diffusivity. Next, to explore the potential implications of low solute

diffusivity on the efficacy of biologic therapy, we determined the effect of nutrient demand on the relationship between solute diffusion in the CEP and NP cell viability by increasing chamber cell density. Finally, we probed the dependence of solute diffusivity on CEP matrix composition using Fourier transform infrared (FTIR) spectroscopy imaging. These FTIR data were used to test the hypothesis that CEPs with low solute diffusivity have greater mineral, collagen, and aggrecan contents than CEPs with high solute diffusivity.

Method

Study design

A key feature of the study was its ability to isolate nutrient supply as the only variable influencing NP cell function. To do this, we used diffusion chambers that mimic the diffusion-limited nutrient environment of the disc *in vivo*. Briefly, NP cells *in vivo* are mainly nourished by nutrients that diffuse through the CEP matrix. Some NP cells are located directly adjacent to the CEP, while those in the center of the lumbar discs may be 8–10 mm from the nearest vertebral capillary. Analogously, NP cells cultured inside the chambers obtain glucose and oxygen that diffuse through human CEPs at the open sides of the chamber (Figure 2). Meanwhile, disc cell metabolites exit by diffusing through the CEPs into the culture medium. Thus, cell survival and function is a balance between the cell density, which dictates nutrient demand[6], and CEP transport properties, which constrain nutrient supply. By culturing a fixed density of cells inside diffusion chambers with CEP tissues that span a physiologic range of transport properties, we determined how differences in transport directly affect NP cell viability and gene expression.

CEP tissues

Intact human CEPs were harvested from six fresh cadaveric lumbar spines (age range: 38–66 years old; mean age: 56 ± 10 years) with no history of musculoskeletal disorders. From each L4 and L5 disc, full-thickness CEP samples (15 mm-wide in the coronal plane), including any calcified cartilage, were removed from either the cranial or caudal subchondral bone adjacent to the NP, flash-frozen in OCT compound (Tissue-Tek; Sakura, Tokyo, Japan), and cryostat-sectioned perpendicular to the CEP surface.

CEP transport properties

The diffusivity of a small solute inside each CEP was measured using fluorescence recovery after photobleaching (FRAP; see Supplementary Material for details). Briefly, full-thickness CEP samples (5 mm-wide in the coronal plane x 2 mm-long in the sagittal plane) site-matched to the tissues used in the diffusion chambers were immersed in PBS containing sodium fluorescein (376 Da), and FRAP was performed with a 25 μm bleach radius (w) at 4–6 cranial-caudal locations per CEP with a confocal microscope (SP5; Leica Microsystems). Diffusivity was calculated using the Axelrod method[23] following a previous procedure[24]. The time constant of recovery (τ) and recovery half-time ($\tau_{1/2}$) were obtained by curve-fitting the normalized fluorescence intensity during recovery to an exponential function (Figure 3), and solute diffusivity was defined as $D = 0.88*w^2/(4\tau_{1/2})$. Sodium fluorescein was studied because its molecular weight is similar to metabolically relevant solutes, *e.g.* glucose (180 Da) and lactate (90 Da).

CEP biochemical composition

CEP biochemical composition was measured spatially with FTIR imaging. CEP sections (7 μm thick) adjacent to those used in the diffusion chambers were mounted on barium fluoride windows (Edmund Optics, Barrington, NJ), air dried for 4 hr, and imaged with a Spotlight 400 microscope (Perkin Elmer, Waltham, MA). Images were acquired in transmittance mode with 4 cm^{-1} spectral resolution and 6.25 μm pixel size. Spatial maps of collagen (1595–1710 cm^{-1} Amide I peak area), aggrecan (960–1185 cm^{-1} carbohydrate peak area), mineral-to-matrix ratio (ratio of phosphate's 895–1215 cm^{-1} P-O stretch peak area to Amide I peak area), and collagen cross-link maturity ratio (ratio of 1660:1690 cm^{-1} peaks; sensitive to the relative amount of mature pyridinoline cross-links to immature, reducible cross-links[25]) were calculated in 0.4 mm *x* 0.8 mm ROIs (one ROI/section). Spectral indices at normalized depths were calculated for three adjacent sections/CEP. We performed this analysis for three CEPs with the highest and lowest diffusivities (6 CEPs total), selected from different donors.

CEP thickness

CEP thickness was measured using photomicrographs and was averaged for five locations/chamber.

NP cell isolation

In order to limit the confounding effects of NP cell heterogeneity, we used bovine NP cells, which are phenotypically similar to human NP cells[26–29]. Additionally, bovine NP cells are derived from discs with similar physico-chemical properties[29,30], they can be acquired in large numbers, and they have less donor-to-donor variability[28,29]. NP cells were isolated from coccygeal discs obtained from three steers (24–28 months old) collected at slaughter from a local abattoir (Marin Sun Farms, Petaluma, CA). Details of the isolation and expansion procedures are included in the Supplementary Material. For the diffusion chamber experiments, NP cells were mixed with agarose (type VII; Sigma-Aldrich) to give a final concentration of 1% agarose and cell densities of 4 million cells/mL, which is the average NP cell density in adult discs[18], and 8 million cells/mL.

Diffusion chambers

The diffusion chambers were a modification of those described previously[6]. Each chamber was comprised of two glass slides separated by impermeable spacers (Figure 2). Two 180 μm-thick sections from each CEP were first washed for 90 min with PBS containing antibiotics (0.012% penicillin, 0.02% streptomycin, 0.01% gentamicin; Sigma-Aldrich) and then placed with the deep layer of the CEP at the open sides of the chambers. Next, the NP cell-agarose mixture was pipetted into the center of the chambers, the chambers were placed in dishes with 25 mL of growth medium, and the dishes were incubated in 21% O_2 for 72 hr at 37°C. Owing to mismatch between CEP section thickness and spacer height, the CEPs sustained a small compressive strain during incubation. This overall setup recapitulated the barrier function of the CEP, which was most relevant to our goals.

Cell viability

Cell viability after incubation was assessed using a cytotoxicity assay (Thermo Fisher Scientific; see Supplementary Material for details). Briefly, gels were co-stained with calcein-AM and ethidium homodimer-1, and imaged using fluorescence microscopy. Low-magnification (1x) images (MZ FLIII; Leica Microsystems, Wetzlar, Germany) were acquired for semi-quantitative analysis of viable distance using the ruler tool in ImageJ (NIH, USA). Viable distance was averaged at three locations/chamber, and experiments were repeated for each CEP and cell density. Viability data from three CEPs were unavailable since the agarose gels associated with those experiments broke apart during processing. Semi-quantitative estimates of viable distance were within 10% of measurements derived from a high-magnification analysis of viable cell percentage.

Gene expression

After chamber incubation, *in situ* hybridization (ISH) was performed to examine anabolic and catabolic gene expression (2 chambers/CEP; 4 million cells/mL). ISH was carried out using the RNAscope Fluorescent Multiplex Assay (Advanced Cell Diagnostics, Newark, CA; see Supplementary Material for details). Briefly, the cell-embedded gels were quartered, and one quarter-gel from each chamber was co-stained with probes for *ACAN* (cat no. 515691) labeled with Cy3, *COL2A1* (cat no. 515711) labeled with Cy5, and *UBC* (cat no. 464851; positive control) labeled with FITC. A second quarter-gel was co-stained with probes for *MMP-2* (cat no. 515701) labeled with Cy3, *HIF1A* (cat no. 515721) labeled with Cy5, and *UBC* labeled with FITC. Processing was performed according to the manufacturer's protocol, and cell nuclei were stained with 4',6-diamidino-2-phenylindole (DAPI).

Stained gels were imaged with a confocal microscope (SP5; Leica Microsystems) using the standard emission/excitation settings for each fluorophore and 40x objective. Images in each channel were taken as a series of z-sections (1.05 μm/section, 512 × 512) spanning a 21 μm-tall zone at the mid-height of the gel. Stacks in this manner were collected at 0.5-mm intervals across the viable region of the quarter-gels (3 scans/quarter-gel). mRNA expression was estimated from the average fluorescence intensity of nuclei-associated pixels[31], which was calculated using a macro in ImageJ. Experiments were performed twice each for chambers with the highest and lowest diffusivity CEPs.

Statistical analysis

Linear regression was used to determine the relationship between our primary outcomes, viable distance and solute diffusivity. The CEPs used in the regression models were derived from the L4 and L5 discs of six donors and were treated as independent samples. This is because there was no pairwise association or agreement between the diffusivities of the L4 and L5 CEPs, and indeed, for a given spine, some discs may degenerate while others do not[32]. We further confirmed sample independence and regression model validity by re-running the models after randomly removing one CEP belonging to each donor. To determine how solute diffusivity affects viable distance when cell density is increased, we separated the CEPs into two groups — one group with the highest diffusivities ($n = 6$ CEPs) and one with the lowest ($n = 5$ CEPs). For each group, we compared the viable distance

between chambers with high and low cell densities using a 2-sample independent *t*-test. These sample sizes were chosen to detect the smallest practical difference in viable distance, 0.45 ± 0.18 mm, with 90% power and a level of 0.05 using a 2-sample *t*-test. In pilot studies, 0.45 mm was the typical 95% confidence interval for the viable distance measurements within a single chamber.

To describe the fluctuations in NP cell gene expression with distance from the CEP, we used a regression model of fluorescence intensity as a function of location, a categorical independent variable. A separate regression analysis resulting in a population average curve for each gene was generated for the chambers with the highest and lowest diffusivity CEPs. We accounted for 8–10 locations nested within each of the three scans/chamber using a mixed effects regression model to account for repeated measures.

To describe the spatial fluctuations in CEP composition, we used regression models of the FTIR indices as a function of normalized depth from the NP/CEP interface, a continuous independent variable. For all of the indices except cross-link maturity (4^{th}-degree polynomial model), a 5^{th}-degree polynomial model for normalized depth was fitted with random intercepts and slopes[33] (see Supplementary Material for details). We tested whether overall trajectories differed by diffusivity status via a post-estimation test using a contrast statement (F-test).

All analyses were performed using JMP Pro 12 and SAS v9.4 (SAS Institute; Cary, NC, USA). $p < 0.05$ (2 tailed) was considered statistically significant. Data are given as mean ± SD.

Results

CEP samples demonstrated large variations in diffusive transport, which in turn, had significant effects on NP cell viability and function. The mean diffusivity of sodium fluorescein in the CEP tissues was 14.8 ± 5.1 $\mu m^2/s$ (range: 5.9–21.5 $\mu m^2/s$), and diffusivity was not significantly correlated with donor age ($p = 0.68$). These diffusivities are about 5% of those found in aqueous solutions[34], indicating low CEP hydration. Importantly, fluorescein diffusivity, which served as a proxy for small solute diffusion, was significantly and positively correlated with viable distance in the diffusion chambers (4 million cells/mL: 0.24; 95% CI: 0.09, 0.39; $p = 0.006$; 8 million cells/mL: 0.06; 95% CI: 0.03, 0.09; $p = 0.003$; Figure 4A). Specifically, for chambers incubated with 4 million cells/mL, the CEPs that allowed the least diffusive transport showed up to 51% shorter viable distance compared to the CEPs that allowed the most transport. CEP transport properties also influenced anabolic and catabolic gene expression by the NP cells within the viable region of the chambers (Figure 5): CEPs that permitted the least transport attenuated the expression of *ACAN* (Figure 5C), *COL2A1* (Figure 5E), and *MMP-2* (Figure 5G). *HIF1A* levels (Figure 5I) were insensitive to differences in transport.

As expected, doubling the cell density decreased the viable distance; however, this effect depended on the transport properties of the CEP. For CEPs that provided high diffusive transport (fluorescein diffusivity >15 $\mu m^2/s$, the median for all CEPs), the average viable

distance was 22.9% shorter in the chambers with the higher cell density (mean difference: 1.59 mm; 95% CI: 0.95, 2.22; $p = 0.0003$; Figure 4B), which is consistent with the increased nutrient demand. However, for CEPs with low diffusivity (<15 $\mu m^2/s$), there was overlap in the relationships between viable distance and diffusivity (Figure 4A). Thus, viable distance was similar between the two cell densities (mean difference: −0.15 mm; 95% CI: −1.05, 0.74; $p = 0.70$; Figure 4B). This suggests that in those cases, the main limiting factor was poor nutrient supply owing to low diffusive transport, not the increased nutrient demand caused by the higher number of cells. CEP thickness (0.680 ± 0.119 mm) was similar to previous values[35,36] and was not significantly correlated with viable distance for chambers with either cell density (4 million cells/mL: $p = 0.39$; 8 million cells/mL: $p = 0.14$).

Biochemical composition differed significantly between CEPs with high *vs.* low solute diffusivity (Figure 6). Compared to the CEPs with high diffusivity (>15 $\mu m^2/s$) that resulted in longer viable distance, the CEPs that allowed only low diffusive transport (<15 $\mu m^2/s$) had overall greater Amide I peak areas (Figure 6C) and carbohydrate peak areas (Figure 6E), higher mineral-to-matrix ratios (Figure 6G), and lower collagen cross-link maturity (Figure 6I). Depth-wise analysis indicated that the differences in Amide I peak area and collagen cross-link maturity depended on depth.

Discussion

Our results show that physiologic fluctuations in human CEP composition and transport directly affect NP cell survival and function. Small solute diffusivity varied nearly 4-fold in our sample, and the CEPs that permitted the least diffusive transport caused reductions in nutrient supply that shortened the viable distance by up to 51% inside diffusion chambers with NP cell density typical of an average adult disc. The CEPs that allowed poor nutrient diffusion also appeared to downregulate anabolic and catabolic gene expression by the NP cells, which suggests that low nutrient diffusion through the CEP limits the number of disc cells that can be sustained and hinders the cells' ability to preserve matrix homeostasis. Importantly, CEP transport properties played a key role in the reduction in viability that occurred when we increased cell density. Increasing cell density is expected to shorten the viable distance by raising nutrient demands[6], but in our system we found that this effect depended on the transport properties of the CEP. Namely, for CEPs with low diffusive transport, viable distance was insensitive to a doubling of the cell density, which suggests that those CEPs may not allow adequate nutrient diffusion to satisfy cellular demands. Since nutrient diffusion through the CEP depends in part on the porosity and composition of the cartilage matrix[37], we used FTIR imaging to identify compositional differences between the CEPs with high *vs.* low diffusivity. Our FTIR data reveal that the low-diffusivity CEPs that shortened the viable distance had greater amounts of collagen and aggrecan, more mineral, and lower cross-link maturity — characteristics that may physically block solute penetration and diffusion. Taken together, these findings suggest that CEP transport properties have significant effects on nutrient supply and NP cell survival/function, and that deficits in CEP matrix composition may prevent adequate nutrient diffusion and could thereby hinder the success of biologic therapies that require increased nutrient supply.

A clinically relevant finding of this study is that the effects of increasing NP cell density depended on CEP transport properties. NP cell metabolism occurs mainly by anaerobic glycolysis[38], and thus, cell survival and function is sensitive to glucose availability[6]. Increasing cell density hastens glucose consumption, which leads to a steeper concentration gradient and a larger non-viable zone[6,39]. The size of this zone also depends on diffusional supply. Here, chambers with CEPs that allowed less diffusion had a larger non-viable zone; for the CEPs that allowed the least diffusion, nutrient supply appeared to be lower than required by the cells at either cell density. One potential implication of this finding is that CEP properties can have a significant impact on the regenerative potential of biologic therapies that, by design, stimulate nutrient demands. Specifically, patients with deficient CEP transport properties may have inadequate nutrient supply and thus be poor candidates for these therapies. A second implication motivates the development of non-invasive screening tools for the CEP that can help identify patients with adequate nutrient supply. For example, quantitative techniques based on ultrashort echo time (UTE) MRI are appealing since the short echo times are needed to capture the CEP signal, and because T2* relaxation times from UTE MRI are sensitive to the relative amounts of collagen and proteoglycan[40], characteristics that were presently found to influence transport properties.

The CEPs that permitted the least diffusive transport negatively affected anabolic and catabolic gene expression of the NP cells, which is consistent with known effects of reduced nutrient supply. Specifically, *ACAN*, *COL2A1*, and *MMP-2* expression were sensitive to reductions in media glucose concentration[41], whereas *HIF1A* expression was insensitive to culture conditions[42]. The consistency of our results with those previous studies supports the validity of the measurements and conclusions. While other anabolic, catabolic, and pro-inflammatory factors are involved in disc degeneration, the relevance of *ACAN* and *COL2A1* attenuation to diminished disc height and biomechanical properties suggests that those functional deficits within the NP may be related in part to poor CEP transport properties.

Our finding that low solute diffusivity was associated with greater amounts of collagen and aggrecan, more mineral, and lower collagen cross-link maturity within CEPs suggests that these characteristics block solute penetration and diffusion. For example, high amounts of collagen and aggrecan hinder solute uptake and diffusion by reducing the available pore space[19,37], and mineral is highly impermeable[18]. Additionally, a lower amount of mature pyridinoline cross-links, which normally increase as cartilage matures[43,44], could destabilize the collagen network. These compositional deficits may serve as targets for treatments aimed at enhancing CEP transport properties to improve disc nutrition. For example, we recently found that treating CEP tissues with human collagenase liberates the matrix constituents that impede solute uptake, thereby improving nutrient diffusion and NP cell viability (under review). Interestingly, we found significant differences in composition between CEPs with low *vs*. high solute diffusivity throughout the depth of the CEP, which suggests that reduced diffusive transport relates to global changes in CEP matrix biosynthesis rather than local changes in any one region. Thus, treatments for enhancing CEP transport properties may need to act over the entire depth of the CEP. This is unlike articular cartilage, which has zones of varying fiber arrangement and matrix composition that undergo distinct changes with osteoarthritis[45]. Although we are unaware of prior studies that report FTIR

characteristics of the CEP, the generality of our findings is supported by observations that the CEP lacks clear zones in fiber arrangement[46], is thinner than articular cartilage, and has higher collagen content[47].

Despite the importance of the CEP for disc nutrition, the molecular mechanisms underlying the matrix changes that impact nutrient diffusion remain unclear. One possible explanation relates to the effects of free calcium on matrix homeostasis. Grant *et al.* found greater calcium content in CEPs adjacent to more severely degenerated discs, and increasing the levels of calcium decreased the secretion of type I/II collagen and proteoglycan in cultured human CEP cells through activation of the extracellular calcium-sensing receptor[21]. Here, the low-diffusivity CEPs had greater mineral-to-matrix ratios and higher levels of collagen, aggrecan, and immature cross-links. We believe these more dense CEPs represent the later 'degeneration/fibrotic' phase of CEP matrix turnover identified by Antoniou *et al.*, which was characterized by an increase in denatured collagen and increased type I collagen synthesis[22]. Conversely, the less dense CEPs in our study are consistent with the earlier 'aging and maturation' phase of turnover, which includes a drop in synthetic activity and a reduction in denatured type II collagen[22]. Additional research is needed to clarify the molecular mechanisms involved in these phases.

One limitation of our study is that we evaluated the effects of CEP transport properties under diffusive conditions that occurred under low magnitude static loading, while higher magnitude static loading or dynamic loading could increase transport via forced solute convection[48]. The role of solute convection in disc nutrition is unclear, but we expect the present data to be representative of the relative effects of CEP transport properties on nutrient supply. A second limitation is that the CEPs were denuded of cells. Studying CEPs with viable chondrocytes may be important in accounting for local nutrient gradients over time or to address changes in CEP matrix turnover. However, we presently sought to take a snapshot of CEP compositional characteristics, and from that identify how variations in those characteristics impact nutrient supply. In this context, we believe the lack of viable chondrocytes, which are estimated to be between 6–10-fold fewer in number compared to NP cells[18,49], is unlikely to change overall conclusions. A third limitation was the small sample size. Although solute diffusivity varied nearly 4-fold and the number of CEPs was sufficient to detect differences in NP cell viability, the CEPs were derived from six donors with narrow age range. A larger sample size with younger and older donors may have greater variations in composition and transport properties, which could increase their roles.

Finally, we focused on the diffusivity of sodium fluorescein, which is larger than metabolically relevant solutes such as glucose and lactate. Consequently, fluorescein diffusivity ($14.8 \pm 5.1\ \mu m^2/s$) was slower than glucose diffusivity measured previously in human CEPs ($34.4 \pm 9.7\ \mu m^2/s$)[37]. Fluorescein diffusivities in the CEP were also slower than fluorescein diffusivities in the annulus fibrosus ($38 \pm 25\ \mu m^2/s$)[50], which is consistent with the lower porosity of the CEP. Collectively, these observations support the validity of the fluorescein diffusivities and their reflection of small solute diffusion in the CEP.

In summary, our findings demonstrate how CEP composition significantly affects NP cell survival and function. CEPs with poor diffusion had compositional deficits that block solute

passage, including greater amounts of collagen and aggrecan, more mineral, and lower cross-link maturity. Moreover, CEP transport deficits had a detrimental effect on viability when cell density was increased. Taken together, these findings show that NP cell survival and function depend on CEP composition, and that deficits in CEP composition could limit the success of biologic therapies that require increased nutrient supply.

Supplementary Material

Refer to Web version on PubMed Central for supplementary material.

Acknowledgements

The authors thank Drs. Xinyan Tang and Misaki Ouchida for assisting with growing the cells and for providing the illustrations.

Role of funding sources

This work was funded by National Institutes of Health grants to AJF (R01 AR070198 and P30 AR066262), a UCSF Pathways to Discovery grant to JW, a North American Spine Society Young Investigator Research Grant to AJF, and pilot grants from the UCSF School of Medicine and UCSF Core Center for Musculoskeletal Biology & Medicine to AJF. This publication was supported by the National Center for Advancing Translational Sciences, National Institutes of Health, through UCSF-CTSI Grant Number UL1 TR001872.

References

1. Kregar Velikonja N, Urban J, Frohlich M, Neidlinger-Wilke C, Kletsas D, Potocar U, et al. Cell sources for nucleus pulposus regeneration. Eur Spine J 2014;23(Suppl 3):S364–374, 10.1007/s00586-013-3106-9. [PubMed: 24297331]
2. Woods BI, Vo N, Sowa G, Kang JD. Gene therapy for intervertebral disk degeneration. Orthop Clin North Am 2011;42:563–574, 10.1016/j.ocl.2011.07.002. [PubMed: 21944592]
3. Bae WC, Masuda K. Emerging technologies for molecular therapy for intervertebral disk degeneration. Orthop Clin North Am 2011;42:585–601, 10.1016/j.ocl.2011.07.004. [PubMed: 21944594]
4. Wang Z, Hutton WC, Yoon ST. ISSLS Prize winner: Effect of link protein peptide on human intervertebral disc cells. Spine 2013;38:1501–1507. [PubMed: 23370687]
5. Gawri R, Antoniou J, Ouellet J, Awwad W, Steffen T, Roughley P, et al. Best paper NASS 2013: link-N can stimulate proteoglycan synthesis in the degenerated human intervertebral discs. Eur Cell Mater 2013;26:107–119, 10.22203/eCM.v026a08. [PubMed: 24027023]
6. Horner HA, Urban JP. 2001 Volvo Award Winner in Basic Science Studies: Effect of nutrient supply on the viability of cells from the nucleus pulposus of the intervertebral disc. Spine 2001;26:2543–2549. [PubMed: 11725234]
7. Huang YC, Urban JP, Luk KD. Intervertebral disc regeneration: do nutrients lead the way? Nat Rev Rheumatol 2014;10:561–566. [PubMed: 24914695]
8. Zhu Q, Gao X, Temple HT, Brown MD, Gu W. Simulation of biological therapies for degenerated intervertebral discs. J Orthop Res 2016;34:699–708. [PubMed: 26425965]
9. Crock HV, Yoshizawa H. The blood supply of the lumbar vertebral column. Clin Orthop Relat Res 1976;115:6–21.
10. Urban JP, Holm S, Maroudas A, Nachemson A. Nutrition of the intervertebral disk. An in vivo study of solute transport. Clin Orthop Relat Res 1977;129:101–114.
11. Fields AJ, Ballatori A, Liebenberg EC, Lotz JC. Contribution of the endplates to disc degeneration. Curr Mol Biol Rep 2018;4:151–160. [PubMed: 30546999]
12. Lotz JC, Fields AJ, Liebenberg EC. The Role of the Vertebral End Plate in Low Back Pain. Global Spine J 2013;3:153–164. [PubMed: 24436866]

13. Aoki J, Yamamoto I, Kitamura N, Sone T, Itoh H, Torizuka K, et al. End plate of the discovertebral joint: degenerative change in the elderly adult. Radiology 1987;164:411–414. [PubMed: 3602378]
14. Rodriguez AG, Rodriguez-Soto AE, Burghardt AJ, Berven S, Majumdar S, Lotz JC. Morphology of the human vertebral endplate. J Orthop Res 2012;30(2):280–287, 10.1002/jor.21513. [PubMed: 21812023]
15. Zehra U, Robson-Brown K, Adams MA, Dolan P. Porosity and Thickness of the Vertebral Endplate Depend on Local Mechanical Loading. Spine (Phila Pa 1976) 2015;40(15):1173–1180, 10.1097/BRS.0000000000000925. [PubMed: 25893360]
16. Rodriguez AG, Slichter CK, Acosta FL, Rodriguez-Soto AE, Burghardt AJ, Majumdar S, et al. Human disc nucleus properties and vertebral endplate permeability. Spine 2011;36:512–520. [PubMed: 21240044]
17. DeLucca JF, Cortes DH, Jacobs NT, Vresilovic EJ, Duncan RL, Elliott DM. Human cartilage endplate permeability varies with degeneration and intervertebral disc site. J Biomech 2016;49:550–557. [PubMed: 26874969]
18. Maroudas A, Stockwell RA, Nachemson A, Urban J. Factors involved in the nutrition of the human lumbar intervertebral disc: cellularity and diffusion of glucose in vitro. J Anat 1975;120(Pt 1):113–130. [PubMed: 1184452]
19. Roberts S, Urban JP, Evans H, Eisenstein SM. Transport properties of the human cartilage endplate in relation to its composition and calcification. Spine 1996;21:415–420. [PubMed: 8658243]
20. Benneker LM, Heini PF, Alini M, Anderson SE, Ito K. 2004 Young Investigator Award Winner: vertebral endplate marrow contact channel occlusions and intervertebral disc degeneration. Spine 2005;30:167–173. [PubMed: 15644751]
21. Grant MP, Epure LM, Bokhari R, Roughley P, Antoniou J, Mwale F. Human cartilaginous endplate degeneration is induced by calcium and the extracellular calcium-sensing receptor in the intervertebral disc. Eur Cell Mater 2016;32:137–151. [PubMed: 27452962]
22. Antoniou J, Goudsouzian NM, Heathfield TF, Winterbottom N, Steffen T, Poole AR, et al. The human lumbar endplate. Evidence of changes in biosynthesis and denaturation of the extracellular matrix with growth, maturation, aging, and degeneration. Spine 1996;21:1153–1161. [PubMed: 8727189]
23. Axelrod D, Koppel DE, Schlessinger J, Elson E, Webb WW. Mobility measurement by analysis of fluorescence photobleaching recovery kinetics. Biophys J 1976;16:1055–1069. [PubMed: 786399]
24. Leddy HA, Guilak F. Site-specific molecular diffusion in articular cartilage measured using fluorescence recovery after photobleaching. Ann Biomed Eng 2003;31:753–760. [PubMed: 12971608]
25. Paschalis EP, Verdelis K, Doty SB, Boskey AL, Mendelsohn R, Yamauchi M. Spectroscopic characterization of collagen cross-links in bone. J Bone Miner Res 2001;16:1821–1828. [PubMed: 11585346]
26. Horner HA, Roberts S, Bielby RC, Menage J, Evans H, Urban JP. Cells from different regions of the intervertebral disc: effect of culture system on matrix expression and cell phenotype. Spine 2002;27:1018–1028. [PubMed: 12004167]
27. Miyazaki T, Kobayashi S, Takeno K, Meir A, Urban J, Baba H. A phenotypic comparison of proteoglycan production of intervertebral disc cells isolated from rats, rabbits, and bovine tails; which animal model is most suitable to study tissue engineering and biological repair of human disc disorders? Tissue Eng Part A 2009;15:3835–3846. [PubMed: 19681728]
28. Minogue BM, Richardson SM, Zeef LA, Freemont AJ, Hoyland JA. Transcriptional profiling of bovine intervertebral disc cells: implications for identification of normal and degenerate human intervertebral disc cell phenotypes. Arthritis Res Ther 2010;12:R22. [PubMed: 20149220]
29. Oshima H, Ishihara H, Urban JP, Tsuji H. The use of coccygeal discs to study intervertebral disc metabolism. J Orthop Res 1993;11:332–338. [PubMed: 8326439]
30. Demers CN, Antoniou J, Mwale F. Value and limitations of using the bovine tail as a model for the human lumbar spine. Spine 2004;29:2793–2799. [PubMed: 15599281]
31. Technical Note: Guideline on how to quantify RNAscope® Fluorescent Assay Results. Advanced Cell Diagnostics, Inc. 2017.

32. Cheung KM, Samartzis D, Karppinen J, Luk KD. Are “patterns” of lumbar disc degeneration associated with low back pain?: new insights based on skipped level disc pathology. Spine (Phila Pa 1976) 2012;37(7):E430–438, 10.1097/BRS.0b013e3182304dfc. [PubMed: 22466575]
33. Laird NM, Ware JH. Random-effects models for longitudinal data. Biometrics 1982;38:963–974. [PubMed: 7168798]
34. Periasamy N, Verkman AS. Analysis of fluorophore diffusion by continuous distributions of diffusion coefficients: application to photobleaching measurements of multicomponent and anomalous diffusion. Biophys J 1998;75:557–567. [PubMed: 9649418]
35. Berg-Johansen B, Han M, Fields AJ, Liebenberg EC, Lim BJ, Larson PE, et al. Cartilage Endplate Thickness Variation Measured by Ultrashort Echo-Time MRI Is Associated With Adjacent Disc Degeneration. Spine (Phila Pa 1976) 2018;43(10):E592–E600, 10.1097/BRS.0000000000002432. [PubMed: 28984733]
36. Roberts S, Menage J, Urban JP. Biochemical and structural properties of the cartilage end-plate and its relation to the intervertebral disc. Spine 1989;14:166–174. [PubMed: 2922637]
37. Wu Y, Cisewski SE, Wegner N, Zhao S, Pellegrini VD Jr., Slate EH, et al. Region and strain-dependent diffusivities of glucose and lactate in healthy human cartilage endplate. J Biomech 2016;49:2756–2762. [PubMed: 27338525]
38. Ishihara H, Urban JP. Effects of low oxygen concentrations and metabolic inhibitors on proteoglycan and protein synthesis rates in the intervertebral disc. J Orthop Res 1999;17:829–835. [PubMed: 10632449]
39. Urban JP, Smith S, Fairbank JC. Nutrition of the intervertebral disc. Spine 2004;29:2700–2709. [PubMed: 15564919]
40. Fields AJ, Han M, Krug R, Lotz JC. Cartilaginous end plates: quantitative MR imaging with very short echo times-orientation dependence and correlation with biochemical composition. Radiology 2015;274:482–489. [PubMed: 25302832]
41. Neidlinger-Wilke C, Mietsch A, Rinkler C, Wilke HJ, Ignatius A, Urban J. Interactions of environmental conditions and mechanical loads have influence on matrix turnover by nucleus pulposus cells. J Orthop Res 2012;30:112–121. [PubMed: 21674606]
42. Risbud MV, Guttapalli A, Stokes DG, Hawkins D, Danielson KG, Schaer TP, et al. Nucleus pulposus cells express HIF-1 alpha under normoxic culture conditions: a metabolic adaptation to the intervertebral disc microenvironment. J Cell Biochem 2006;98:152–159. [PubMed: 16408279]
43. Masahiko T, Damle S, Penmatsa M, West P, Yang X, Bostrom M, et al. Temporal changes in collagen cross-links in spontaneous articular cartilage repair. Cartilage 2012;3:278–287. [PubMed: 23272271]
44. Bank RA, Verzijl N, Lafeber FP, Tekoppele JM. Putative role of lysyl hydroxylation and pyridinoline cross-linking during adolescence in the occurrence of osteoarthritis at old age. Osteoarthritis Cartilage 2002;10:127–134. [PubMed: 11869072]
45. Saarakkala S, Julkunen P, Kiviranta P, Makitalo J, Jurvelin JS, Korhonen RK. Depth-wise progression of osteoarthritis in human articular cartilage: investigation of composition, structure and biomechanics. Osteoarthritis Cartilage 2010;18:73–81. [PubMed: 19733642]
46. Paietta RC, Burger E, Ferguson VL. Mineralization and collagen orientation throughout aging at the vertebral endplate in the human lumbar spine. J Struct Biol 2013;184(2):310–320. [PubMed: 23999190]
47. Fields AJ, Rodriguez D, Gary KN, Liebenberg EC, Lotz JC. Influence of biochemical composition on endplate cartilage tensile properties in the human lumbar spine. J Orthop Res 2014;32:245–252. [PubMed: 24273192]
48. Sampson SL, Sylvia M, Fields AJ. Effects of dynamic loading on solute transport through the human cartilage endplate. J Biomech 2018, 10.1016/j.jbiomech.2018.12.004.
49. Liebscher T, Haefeli M, Wuertz K, Nerlich AG, Boos N. Age-related variation in cell density of human lumbar intervertebral disc. Spine (Phila Pa 1976) 2011;36(2):153–159, 10.1097/BRS.0b013e3181cd588c. [PubMed: 20671592]
50. Travascio F, Jackson AR, Brown MD, Gu WY. Relationship between solute transport properties and tissue morphology in human annulus fibrosus. J Orthop Res 2009;27:1625–1630. [PubMed: 19489044]

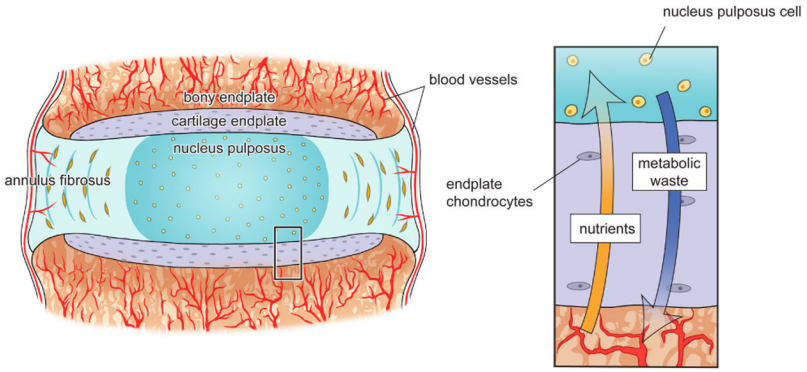

Figure 1:

Vertebral capillaries penetrate the bony endplate and terminate at the cartilage endplate, which forms a continuous interface superior and inferior to the intervertebral disc that separates the vertebra from the inner annulus fibrosus and gelatinous nucleus pulposus. Once nutrients reach the cartilage, small solutes such as glucose and oxygen diffuse in through the cartilage matrix along a steep concentration gradient, while metabolic waste produced by the disc cells, such as lactate, diffuses out (inset).

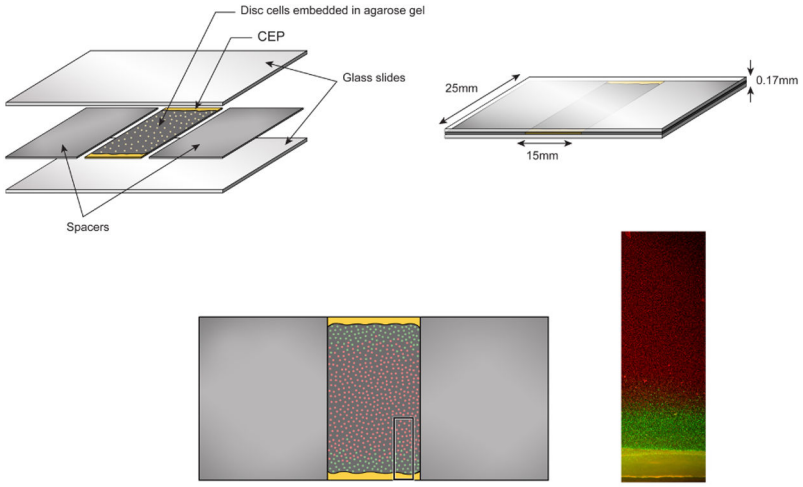

Figure 2:

The diffusion chambers consist of glass slides separated by 170 μm-tall spacers. Nucleus pulposus cells embedded in agarose gel obtain nutrients from their culture medium outside the chambers via diffusion through full-thickness human CEP sections. Following incubation for 72 hr, gels were stained to assess viability (live/dead photomicrograph, inset) and gene expression.

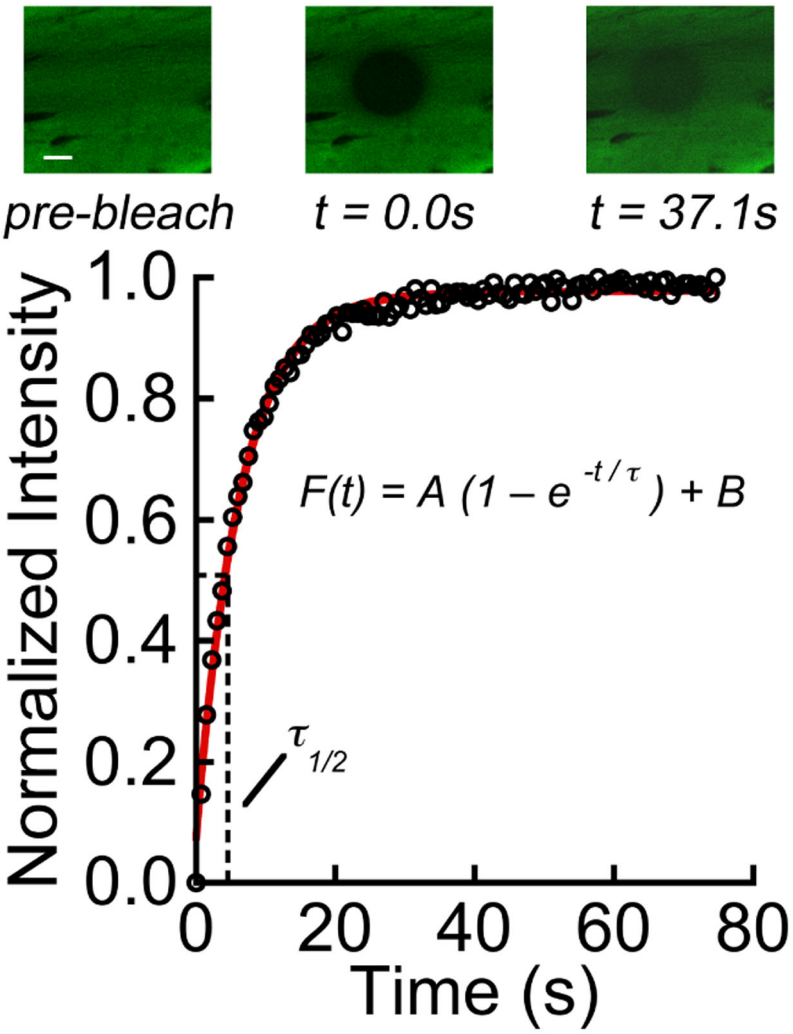

Figure 3:

Upper panel showing photobleaching and fluorescence recovery for CEP tissue. The scale bar indicates 20 μm. Fluorescence intensity in the bleach spot was normalized to pre-bleach intensity, and the resulting normalized intensity values, *F(t)*, were fitted to an exponential recovery curve to determine the time constant of recovery (τ) and recovery half-time ($\tau_{1/2}$). Solute: sodium fluorescein (376 Da).

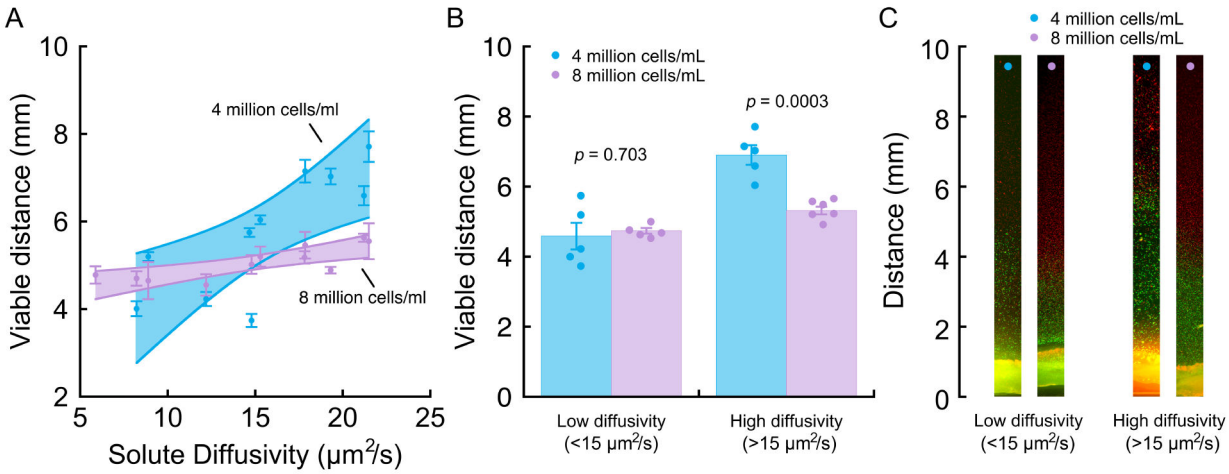

Figure 4:

(A) Viable distance in the diffusion chambers correlated significantly with diffusive transport in the CEPs (determined for sodium fluorescein) at the open sides of the chamber. 4 million cells/mL: for every 1 μm^2/s increase in solute diffusivity, there was a 0.24 mm (95% CI: 0.09–0.39 mm, $p = 0.006$) increase in viable distance ($r^2 = 0.64$, $p = 0.006$); 8 million cells/mL: for every 1 μm^2/s increase in solute diffusivity, there was a 0.06 mm (95% CI: 0.03–0.09 mm, $p = 0.003$) increase in viable distance ($r^2 = 0.65$, $p = 0.003$). Error bars denote estimated mean ± SD calculated from 3 viable distance measurements per CEP and per cell density; the validity of the measurements was confirmed in repeat experiments performed using neighboring tissue sections from the same CEP. For the low chamber cell density, data from 10 different CEPs were used to fit the regression. For the high cell density, data from 11 different CEPs were used. Shaded bands display 95% point-wise CI for each relationship. Solute diffusivity measurements represent the mean from 4–6 measurements repeated at various cranial-caudal locations in each CEP. **(B)** For CEPs with low solute diffusivity, the viable distance in the diffusion chambers was similar for chambers with 4 million cells/mL vs. 8 million cells/mL. For CEPs with high diffusivity, the viable distance was significantly shorter for chambers with 8 million cells/mL. **(C)** Representative low-magnification photomicrographs of live/dead-stained gels from diffusion chambers in each of the groups in panel (B). The same low-diffusivity CEP or high-diffusivity CEP is shown for each group.

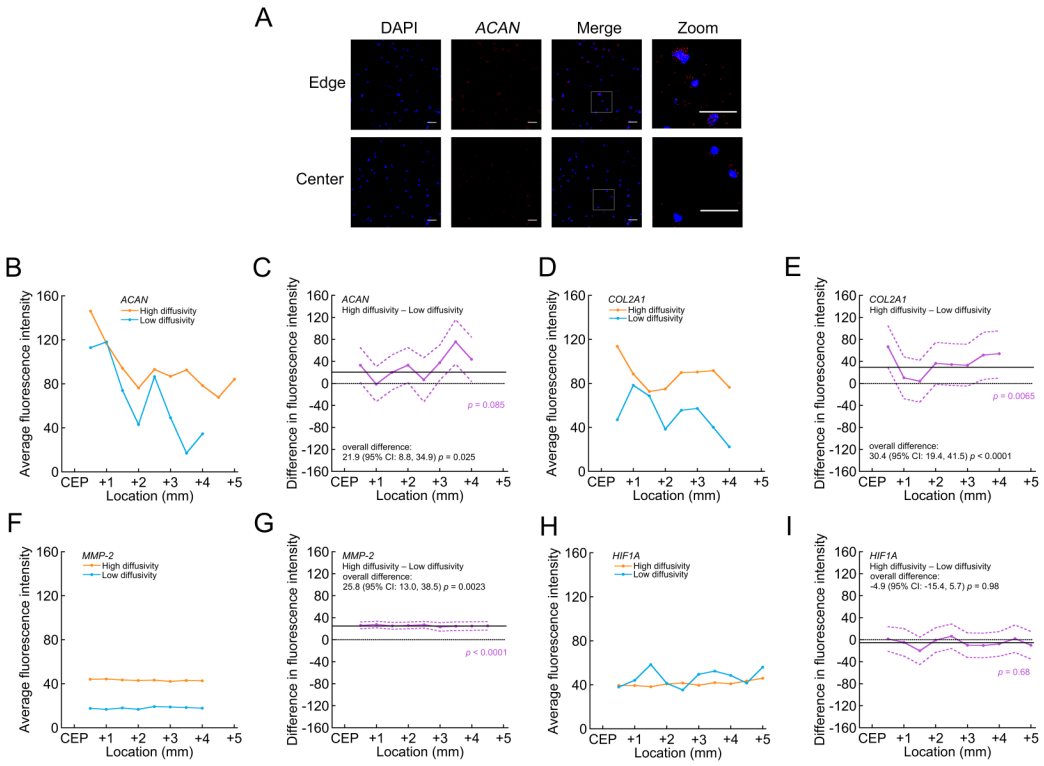

Figure 5:

Comparison of NP cell gene expression in the viable region between diffusion chambers incubated with the highest *vs.* lowest diffusivity CEPs (4 million cells/mL). **(A)** Representative projection images showing *ACAN* localization (red) to cell nuclei (DAPI, blue) near the open edge and center of a diffusion chamber with a high-diffusivity CEP. Boxes indicate the regions of the zoomed insets. Scale bars represent 40 μm. **(B), (D), (F) & (H)** Average fluorescence intensity indicating mRNA expression levels for image stacks acquired at various locations within the viable region of the chambers. Data points show the mean intensity for three scans across two diffusion chambers with the highest diffusivity CEP (21.5 $\mu m^2/s$) and the lowest diffusivity CEP (5.9 $\mu m^2/s$). For both high- and low-diffusivity CEPs, average mRNA levels of *ACAN* **(B)** and *COL2A1* **(D)** appeared to decrease with increasing distance from the CEP, whereas average mRNA levels of *MMP-2* **(F)** and *HIF1A* **(H)** appeared stable. **(C), (E), (G) & (I)** Difference in average fluorescence intensity (purple, with 95% confidence intervals) at various locations indicating difference in mRNA expression levels between chambers with the highest and lowest diffusivity CEPs (high minus low; > zero suggested higher mRNA levels in the chambers with the high-diffusivity CEP). Solid black lines indicate overall difference (*i.e.* for all locations pooled), and dotted black lines indicate no difference. *p*-values in purple indicate statistical significance of the difference between high- and low-diffusivity CEPs as a function of location, and *p*-values in black indicate statistical significance of the overall difference. Overall, compared to chambers with the low-diffusivity CEP, chambers with the high-diffusivity CEP had greater mRNA levels of *ACAN* **(C)**, *COL2A1* **(E)**, and *MMP-2* **(G)**, and similar levels of *HIF1A* **(I)**.

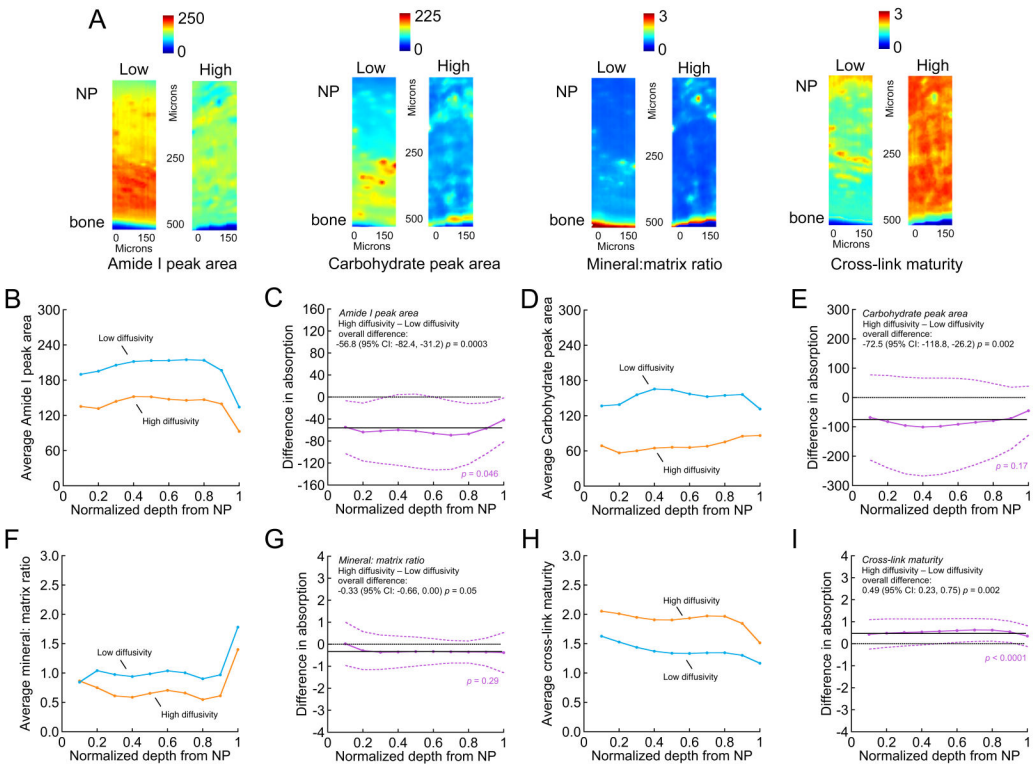

Figure 6:

Comparison of FTIR absorption data between high-diffusivity *vs.* low-diffusivity CEPs. **(A)** Representative absorption maps of Amide I peak area (1595–1710 cm^{-1}, estimate of collagen content), carbohydrate peak area (960–1185 cm^{-1}, estimate of aggrecan content), phosphate (895–1215 cm^{-1}): Amide I peak ratio (indicative of mineral-to-matrix ratio), and 1660:1690 cm^{-1} peak ratio (estimate of collagen cross-link maturity) from high-diffusivity ("High") and low-diffusivity ("Low") CEPs. **(B), (D), (F) & (H)** Average FTIR absorption as a function of normalized depth from the NP/CEP interface. Data points show the mean absorption for high-diffusivity CEPs (>15 $\mu m^2/s$; $n = 3$ CEPs and 3 sections/CEP) and low-diffusivity CEPs (<15 $\mu m^2/s$ $n = 3$ CEPs and 3 sections/CEP). In general, low-diffusivity and high-diffusivity CEPs showed similar depth-wise fluctuation in absorption profiles (*i.e.* parallel lines) for Amide I peak area **(B)** carbohydrate peak area **(D)**, mineral-to-matrix ratio **(F)**, and cross-link maturity **(H)** throughout the thickness of the CEP. **(C), (E), (G) & (I)** Difference in average absorption (purple, with 95% confidence intervals) as a function of normalized depth from the NP/CEP interface between high-diffusivity *vs.* low-diffusivity CEPs (high minus low; > zero suggested higher absorption in the high-diffusivity CEPs). Solid black lines indicate overall difference (*i.e.* for all depths pooled), and dotted black lines indicate no difference. *p*-values in purple indicate statistical significance of the difference between high- and low-diffusivity CEPs as a function of depth, and *p*-values in black indicate statistical significance of the overall difference. Overall, compared to the high-diffusivity CEPs, the low-diffusivity CEPs had significantly greater Amide I peak area **(C)** and carbohydrate peak area **(E)**, higher mineral-to-matrix ratio **(G)**, and lower collagen cross-link maturity **(I)**.